Tectonophysics 493 (2010) 285–296

Contents lists available at ScienceDirect

Tectonophysics

journal homepage: www.elsevier.com/locate/tecto

Supershear Mach-waves expose the fault breakdown slip

Víctor M. Cruz-Atienza [a,*], Kim B. Olsen [b,1]

[a] Universidad Nacional Autónoma de México, Instituto de Geofísica, Departamento de Sismología. Circuito de la Investigación Científica s/n, Ciudad Universitaria, 04510, México D.F., Mexico
[b] Department of Geological Sciences, GMCS 231 MC-1020, 5500 Campanile Drive, San Diego State University, San Diego, CA 92182-1020, United States

ARTICLE INFO

Article history:
Received 23 December 2009
Received in revised form 9 April 2010
Accepted 16 May 2010
Available online 2 June 2010

Keywords:
Supershear rupture propagation
Mach waves
Breakdown slip
Fault friction
Denali
Izmit earthquakes

ABSTRACT

Mikumo et al. (2003) showed that it is possible to estimate the breakdown slip (D_c) as the slip at the time of the peak slip rate for rupture propagation with subshear speeds. Cruz-Atienza et al. (2009) later attempted to extend this method to extract information about D_c as the displacement at the time of the peak particle velocity from seismic strong-motion records. However, a reasonably accurate estimate of D_c was only possible in a narrow zone adjacent to the fault (typically on the order of hundreds of meters) due to the fast decay with distance from the fault of the seismic energy related to the stress breakdown process. When the rupture propagates with supershear-speeds, on the other hand, this energy is carried much farther away from the fault by Mach waves, in particular Rayleigh Mach waves when rupture reaches the Earth's surface (Dunham and Bhat, 2008). Here, we present a new approach to estimate D_c from strong-motion records containing Mach waves. First, we show that the method by Mikumo et al. is valid for supershear rupture propagation. This method is then used to estimate D_c via an asymptotic approximation of the slip and slip-rate time histories from the Mach waves. Using spontaneous rupture simulations we demonstrate that, for a visco-elastic half-space model, D_c can be estimated within an error of 40% from Mach waves that have propagated a distance of at least 3 km from the fault. The method is applied to estimate D_c for the 2002 M_w7.9 Denali, Alaska, earthquake (~1.5 m) and for the 1999 Mw7.6 Izmit, Turkey, earthquake (~1.7 m).

1. Introduction

During an earthquake, changes in stresses on the fault and within the surrounding material occur as the fault slips and radiates seismic waves. The radiated energy strongly depends on the way fault tractions evolve close to the rupture front, where most of the dissipative mechanisms concentrate. Thus, any constraints obtained from observations on how tractions drop as the fault slips are crucial for understanding the rupture process and the generation of reliable physics-based model predictions. One of the most important parameters controlling the traction drop is the breakdown slip, D_c, which is defined as the slip required by the shear traction to progress from its peak value to its residual value during rupture propagation (e.g. Ohnaka et al., 1987; Freund, 1998). A series of studies have tried to estimate D_c from historical earthquakes in order to obtain such constraints. Most of the procedures for these studies were based on indirect source observations reconstructing the fault traction evolution from kinematic source models obtained by inversion of strong-motion seismograms (e.g. Ide and Takeo, 1997; Pulido and Irikura, 2000; Mikumo and Yagi, 2003). However, due to the limited bandwidth of the recorded seismograms used in the inversion, D_c was poorly resolved in these studies. Moreover, dynamic models based on the inferred D_c values may be biased and not able to resolve the stress breakdown process over the fault (Guatteri and Spudich, 2000; Spudich and Guatteri, 2004; Piatanesi et al., 2004).

A somewhat different approach to estimate D_c was introduced by Mikumo et al. (2003) as the slip at the time of the peak slip-rate (D_c') from dynamic rupture simulations. Fukuyama and Mikumo (2007) then proposed to extend this method beyond the fault plane by estimating a parameter, here referred to as D_c'', directly from off-fault strike-parallel seismograms. However, as recently shown by Cruz-Atienza et al. (2009), for subshear rupture conditions (i.e. rupture velocity, v_r, smaller than the S-wave propagation speed, v_s) D_c'' represents a reasonable approximation of D_c only in very specific cases. These authors showed that estimation of D_c from strong-motion records requires a sufficiently wide source spectrum for the breakdown frequencies, fc, to be preserved in the seismograms. These frequencies correspond to the inverse of the breakdown periods, t_c, defined as the time required by the shear fault strength to go from its peak value, $\tau_s = \sigma_n \mu_s$, to its residual value, $\tau_d = \sigma_n \mu_d$, during rupture propagation (σ_n is the normal fault traction, and μ_s and μ_d are the static and dynamic friction coefficients, respectively). Cruz-Atienza et al. concluded that only if rupture reaches the ground surface and within a narrow region adjacent to the fault (where the width is comparable to the fault cohesive zone width, typically on the

* Corresponding author. Tel.: +52 55 56 22 41 26x140; fax: +52 55 56 16 25 47.
E-mail addresses: cruz@geofisica.unam.mx (V.M. Cruz-Atienza), kbolsen@sciences.sdsu.edu (K.B. Olsen).
[1] Tel.: +1 619 594 2649; fax: +1 619 594 4372.

0040-1951/$ – see front matter © 2010 Elsevier B.V. All rights reserved.
doi:10.1016/j.tecto.2010.05.012

order of a few hundred meters), D_c'' is a sufficiently accurate proxy of D_c. These limitations prevent the estimation of D_c directly from strong motion records for most historical earthquakes, and are primarily due to the rapid decay of the high frequencies with distance from the fault when rupture propagates with subshear speeds.

A much different decay of high frequencies is observed for the waves radiated from supershear rupture propagation as compared to earthquakes in the subshear regime (e.g. Bernard and Baumont, 2005; Dunham and Archuleta, 2005; Dunham and Bhat, 2008). If a supershear rupture reaches the Earth's surface both shear and Rayleigh Mach waves are radiated. While shear Mach waves decay as the inverse of the square-root of the propagation distance, Rayleigh Mach waves suffer no attenuation in a loss-less medium. As a consequence, when $v_r > v_s$, high frequencies propagate more efficiently from the source into the far-field as compared to the subshear rupture case (Bizzarri and Spudich, 2008). For this reason, it is possible that breakdown frequencies travel sufficiently far from fault segments with supershear rupture propagation to be captured in strong-motion records of real earthquakes.

Supershear rupture propagation was predicted theoretically more than 30 years ago (Burridge, 1973; Andrews, 1976; Das and Aki, 1977), while the first inferences directly from real earthquakes were made by Archuleta (1984) in records of the 1979 Imperial Valley, CA, earthquake. More recent studies have found additional evidence of supershear rupture propagation from dynamic modeling of records from historical earthquakes and from laboratory experiments (Olsen et al., 1997; Rosakis et al., 1999; Bouchon et al., 2001; Bouchon et al., 2002; Bouchon and Vallée, 2003; Dunham and Archuleta, 2004; Ellsworth et al., 2004; Aagaard and Heaton, 2004; Xia et al., 2005; Das, 2007; Vallée et al., 2008). These studies suggest that supershear rupture transients in real earthquakes arise more often than was presumed a few decades ago. Recent observations indicate that supershear rupture tends to occur along fault segments with simple (i.e., near-planar) geometry and uniform friction (Das, 2007; Bouchon and Karabulut, 2008). Other findings indicate that heterogeneities in the initial fault tractions have little effects on the frequency content of recorded strong motions of Mach waves at a given distance from the fault (Bizzarri et al., 2009).

In this work we study the possibility of estimating the breakdown slip (i.e. the slip weakening distance, D_c) by reconstructing fault-kinematic functions from Mach waves recorded up to several kilometers from the fault. We consider spontaneous-rupture propagation on strike-slip faults that break the surface of three-dimensional (3D) elastic and visco-elastic half-spaces where rupture is governed by slip-weakening friction. First, we show that the method proposed by Mikumo et al. (2003) can be used to accurately estimate D_c for super-shear rupture propagation. We then demonstrate that direct extension of this method to strike-parallel Mach wave particle velocities and displacements does not provide reasonable estimates of D_c. Instead, we discuss the use of an asymptotic representation formula which, applied to recorded Mach waves, leads to an approximation of the slip and slip-rate functions on specific fault segments. We determine as well the accuracy of the resulting D_c estimates as a function of propagation distance. Finally, we apply our approach to estimate D_c using strong-motion records obtained from the 1999 M_w7.6 Izmit and the 2002 M_w7.9 Denali events along segments of the faults where rupture is believed to have propagated with supershear speeds.

2. Experimental setup

The theoretical analysis presented throughout this work is based on numerical results obtained from 3D spontaneous supershear rupture scenarios. These scenarios are simulated with the staggered-grid split-node (SGSN) dynamic rupture method (Dalguer and Day, 2007) using a fourth-order finite difference code (Olsen et al., 2009). Our approach includes a flat free-surface (Gottschaemmer and Olsen, 2001) at the top and perfectly matched layers (PML) absorbing boundaries along all other external edges of the model (Marcinkovich and Olsen, 2003). All simulations correspond to vertical right-lateral strike-slip faults reaching the free surface of elastic or viscoelastic media. The geometry of the problem is shown in Fig. 1. In order to study the radiated energy from ruptures with supershear speeds, the fault length, L, is taken to be much larger than the fault width, W, (i.e. $L \gg W$). In this way, the fracture mode II, where supershear rupture can be generated, dominates the rupture process. If not specified otherwise, the physical dimensions of the vertical fault through all this work are 6 km (width) and 60 km (length). Rupture initiates in a square region of dimensions W by W centered at a depth of $0.5W$ and a distance of $0.5W$ from the left edge of the fault. Strong barriers prevent the spontaneous rupture to propagate beyond the predefined fault area. If not specified otherwise, the elastic properties of the medium are $v_s = 3464$ m/s and $v_p = 6000$ km/s for the S-wave and P-wave velocities, respectively, and $\rho = 2670$ kg/m^3 for the density. We assume a linear slip-weakening constitutive relationship on the fault, which is a simple but well-rooted friction model derived from both experimental observations and theoretical considerations (Ida, 1972; Palmer and Rice, 1973; Andrews, 1976; Ohnaka and Yamashita, 1989; Matsu'ura et al., 1992). Such friction model has been applied by many seismologists to study earthquakes (e.g. Day, 1982; Virieux and Madariaga, 1982; Ide and Takeo, 1997; Olsen et al., 1997; Madariaga et al., 1998; Peyrat et al., 2001; Cruz-Atienza and Virieux, 2004; Cruz-Atienza et al., 2007; Olsen et al., 2008; Olsen et al., 2009), and has three constitutive parameters defining the friction behaviour on the fault: the static (μ_s) and dynamic (μ_d) coefficients of friction, and the slip-weakening distance (i.e. breakdown slip), D_c. To guarantee numerical convergence and stability of our solutions, all rupture simulations were computed considering a grid-size of 50 m, ensuring at least 10 grid points within the stress breakdown zone, for the minimum D_c considered. Simulations were carried out on a 104-processor parallel computer cluster, Pohualli, at the Institute of Geophysics of the National University of Mexico (UNAM).

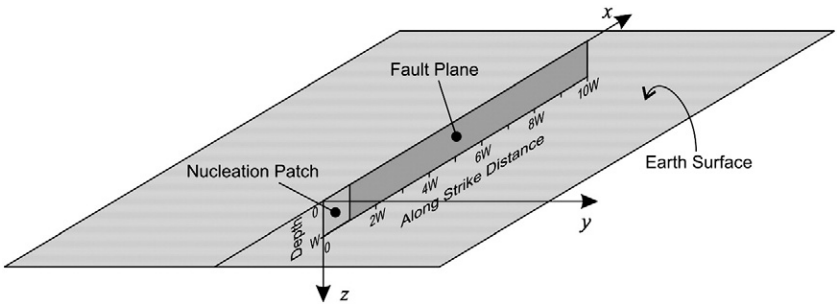

Fig. 1. Problem geometry for our numerical simulations. The vertical strike-slip fault extends from the free surface to a depth (width) of W, with a distance of $10W$ along strike (defined as the x direction). Rupture is nucleated in a small patch with dimensions of $0.5W$ by $0.5W$, centered at a depth of $0.5W$ and a distance of $0.5W$ from the left edge of the fault.

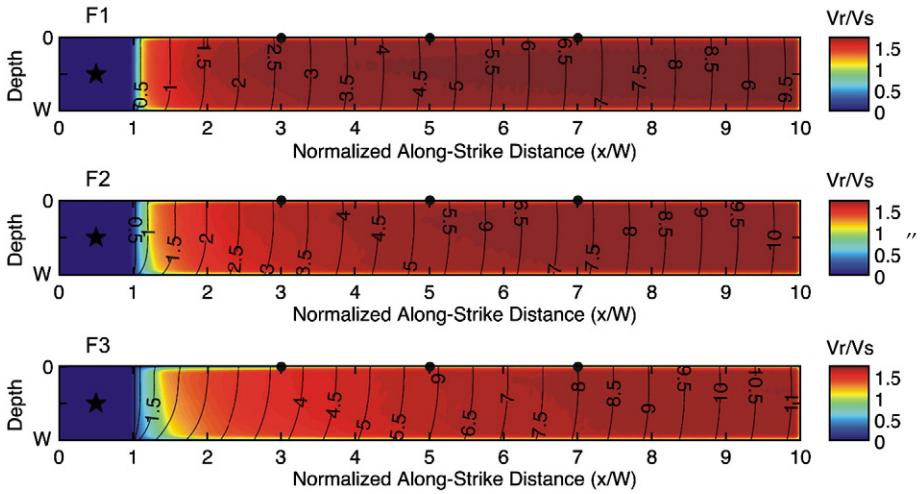

Fig. 2. Rupture velocity (v_r) relative to shear-wave speed (v_s) along with the rupture time contours every 0.5 s over the fault plane for the three rupture cases F1–F3.

3. Stress-breakdown times from supershear slip-rates

The method proposed by Mikumo et al. (2003) to estimate the critical slip-weakening distance D_c on earthquake faults is independent of both fracture and radiated seismic energy. The procedure assumes that the peak slip-rate on a given fault point coincides with the corresponding stress-breakdown time, the time at which the fault strength reaches the residual dynamic level (τ_d), and defines D_c' as the corresponding slip value. Mikumo et al. demonstrated that D_c' is a good proxy of D_c for subshear rupture propagation with heterogeneous stress-drop distributions except at locations near strong barriers and the fault edges. In this section we show that even under supershear conditions, D_c' provides a reasonable approximation to the fault-constitutive breakdown slip D_c.

3.1. Effects on D_c' of changes in D_c

In the following we initially consider three rupture scenarios (F1–F3) with supershear speeds. The only difference between the scenarios is the prescribed homogeneous D_c value on the fault (0.4 m for model F1; 0.8 m for model F2; and 1.2 m for model F3). The constant initial shear and normal fault-tractions are $\tau_0 = 78$ MPa and $\sigma_0 = 120$ MPa, respectively, and the coefficients of static and dynamic friction are $\mu_s = 0.677$ and $\mu_d = 0.525$, respectively. These parameters imply a constant dynamic stress drop equal of $\Delta\tau = 18.6$ MPa. Rupture is nucleated by imposing a value inside the nucleation patch of τ_0 0.36 MPa higher than elsewhere on the fault. Fig. 2 shows the rupture velocity normalized to the constant S-wave speed along with the rupture time contours on the fault for the three rupture cases. For all scenarios, a steady regime with supershear speed is reached after an along-strike rupture distance of about 3W. This distance becomes slightly longer as D_c is increased due to the fact that the fracture energy, G_c, for F2 and F3 is 2 and 3 times bigger, respectively, than its value for F1. Other consequences of the difference in the energy budget are the total rupture time, which increases from about 9.5 s for F1 to about 11 s for F3, and the curvature of the rupture front, which increases with increments in G_c.

To determine the accuracy of estimating the breakdown slip using the method of Mikumo et al. (2003) in the presence of supershear rupture propagation we computed D_c' values throughout the fault for scenarios F1–F3. Fig. 3 shows D_c' estimates normalized by the corresponding prescribed values of D_c along strike-parallel profiles on the fault from the earth surface to a depth of 0.7W for the three scenarios. Overall, the results show very limited dependence of D_c' on the along-strike propagation distance and depth. This result is remarkable considering that the peak slip-rate increases asymptotically along strike. For example, at a depth of 1 km, the peak slip-rate increases from 10 m/s to 15 m/s between along-strike distances of 3W to 10W in the rupture direction for F2 (not shown). Compared to the prescribed fault constitutive values, the D_c' estimates are very close for F2, but overestimate (~20%) and underestimate (~15%) for F1 and F3, respectively. These results suggest that despite significant (up to ~50%) variations in the peak slip-rate on the fault, the stress-breakdown times remain remarkably close to the times of the peak slip-rates.

Two additional tests were carried out to examine the relation between D_c and D_c' in the presence of a sharp, along-dip discontinuity of the prescribed D_c value, separating the fault plane in two areas with constant but different D_c. In case H1, D_c is prescribed to be 0.4 m up to a distance of 5.5W from the nucleation, and 0.8 m at distances between 5.5W and 10W from the nucleation. Case H2 is the same as case H1, except the values of D_c are interchanged between the two areas on the fault. Fig. 4 shows the D_c' estimates at along-strike profiles

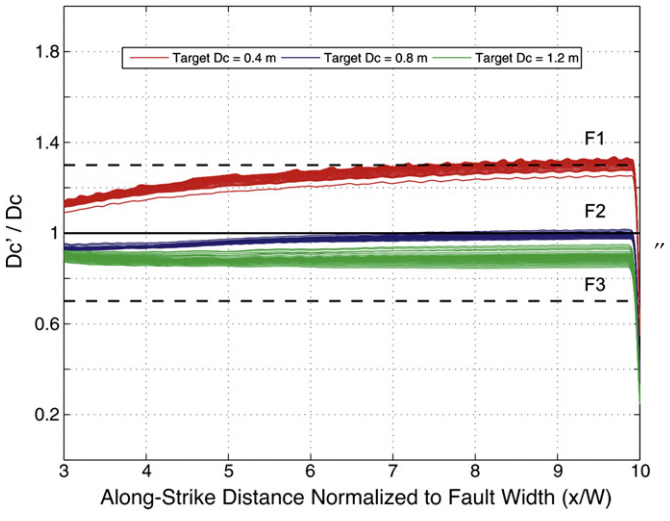

Fig. 3. Estimates of D_c'/D_c ratios for rupture cases F1 (red curves, $D_c = 0.4$ m), F2 (blue curves, $D_c = 0.8$ m) and F3 (green curves, $D_c = 1.2$ m) estimated along strike-parallel profiles on the fault from the earth surface to a depth of 0.7W.

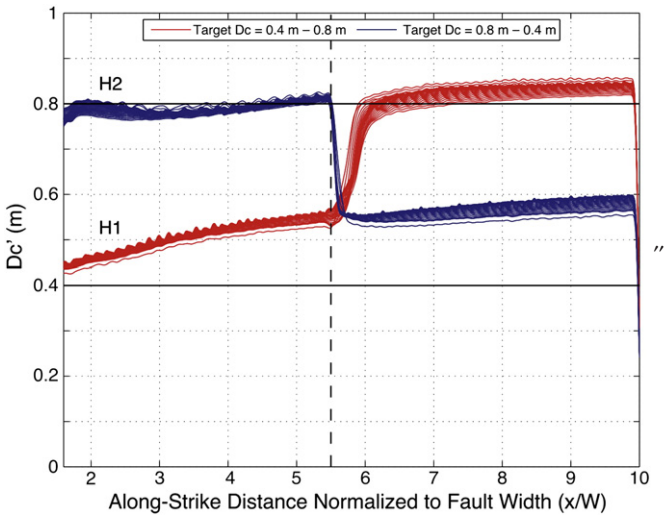

Fig. 4. Estimates of D_c' for rupture cases H1 (red curves), and H2 (blue curves) estimated along strike-parallel profiles on the fault from the earth surface to a depth of 0.7W for a fault with a sharp along-dip separation of two areas with constant D_c (vertical dashed line). In case H1, D_c is 0.4 m for distances up to 5.5W from the nucleation, and 0.8 m for distances beyond 5.5W from the nucleation. Case H2 is the same as case H1, except that the values of D_c are interchanged between the two areas on the fault. The prescribed values of D_c for the two scenarios are depicted by the solid black lines.

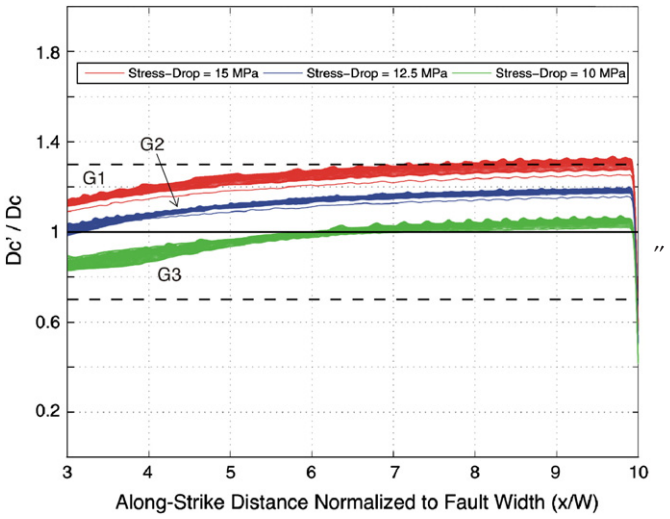

Fig. 5. Estimates of D_c'/D_c ratios (where $D_c = 0.4$ m) for rupture cases G1 (green curves, $\Delta\tau = 10$ MPa), F2 (blue curves, $\Delta\tau = 12.5$ MPa) and F3 (red curves, $\Delta\tau = 15$ MPa) estimated along strike-parallel profiles on the fault from the earth surface to a depth of 0.7W.

for H1 and H2. The prescribed values of D_c are resolved within 50% everywhere on the fault except within a transition zone between the two areas of constant D_c, which for both H1 and H2 is narrower than 0.5W. The width of this zone is largest for H2 where G_c increases as the rupture crosses the transition zone for D_c. Thus, D_c is resolved with almost the same accuracy as that found for faults with constant constitutive parameters, as discussed earlier. We conclude as well that D_c' is quite sensitive to sharp discontinuities of D_c, at least for the values of D_c between 0.4 m and 1.2 m tested here.

3.2. Effects of the dynamic stress drop on D_c'

The F1–F3 cases discussed above assume that the fracture energy (G_c) varies as well as D_c between the scenarios. However, numerical results obtained by Fukuyama et al. (2003) and Cruz-Atienza et al. (2009) show that D_c' is essentially insensitive to changes in G_c. On the other hand, Cruz-Atienza et al. demonstrated that variations in the dynamic stress drop $\Delta\tau$ can have important implications for the radiated wavefield when rupture propagates at subshear speeds. For this reason we estimated D_c' for three additional supershear rupture simulations, with varying $\Delta\tau$ (G1, $\Delta\tau = 10$ MPa; G2, $\Delta\tau = 12.5$ MPa; and G3, $\Delta\tau = 15$ MPa), and constant D_c (equal to 40 cm). Fig. 5 shows normalized D_c' estimates along strike-parallel profiles on the fault from the earth surface to a depth of 0.7W for scenarios G1–G3. All D_c' estimates are within 35% of the prescribed D_c value, while D_c' and $\Delta\tau$ show some limited correlation. We conclude that D_c' is mostly insensitive to variations of the dynamic stress drop $\Delta\tau$.

4. Connection between ground motion and fault mechanics during supershear ruptures

Our numerical experiments discussed above show that D_c may be approximated within 35% by D_c' using slip and slip-rate functions from supershear ruptures in the absence of sharp along-dip variations of D_c. However, this result is of limited practical use, unless it applies to off-fault strong motion records of Mach waves. Cruz-Atienza et al. (2009) showed that for subshear rupture propagations, it is possible to estimate D_c' from D_c'', the latter defined as the rake-parallel displacement field at the peak particle velocity on the free surface, although constrained to a narrow zone adjacent to the fault. In the following we examine to which extent D_c'' is a reasonable proxy of the slip-weakening friction parameter D_c over the fault region where the Mach wave isochrons are located, aided by an asymptotic transformation.

4.1. Characteristics of the wavefield from supershear ruptures

Fig. 6 shows a plan view of our source model along with a schematic representation of the Mach wavefront and the receiver lines where synthetic seismograms are extracted for analysis. The critical angle θ, which is the take-off angle of the Mach wave, determines the ray-parallel direction and is given by $\cos\theta = v_s/v_r$. The faster the rupture speed, the larger the angle θ. The critical point A corresponds to the point on the fault where the Mach wave with the first arrival time at P is generated. We have computed fault-parallel seismograms at the free surface along three receiver lines L1, L2 and L3, for the three rupture cases F1, F2 and F3 (see Fig. 2). We recall that the only fault parameter differing among rupture scenarios F1–F3 is

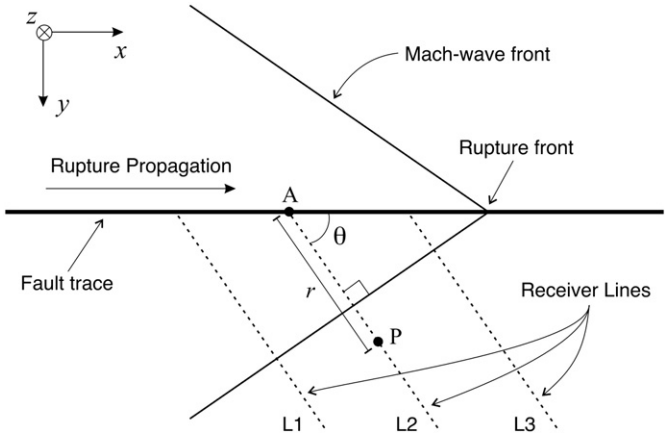

Fig. 6. Plan view of the layout for our Mach wave model. θ depicts the take-off angle of the Mach wave, and the critical point A corresponds to the point on the fault where the Mach wave with the first arrival time at P is generated. L1, L2 and L2 depict receiver lines located at distances of 3W, 5W and 7W from the epicenter.

D_c. The along-strike distances to the receiver lines from the nucleation area (i.e. from $x=0$) are $3W$, $5W$ and $7W$ (black points, Fig. 2). The take-off angles associated with each receiver line are computed from v_r at the corresponding critical points as $\theta_{F1}=[52.8°, 53.2°, 53.3°]$, $\theta_{F2}=[51.2°, 52.5°, 52.8°]$ and $\theta_{F3}=[47.5°, 51.0°, 52.1°]$. As expected, the greater D_c (i.e. G_c), the smaller v_r and θ. 14 receivers at the free surface are considered along each receiver line. The spacing of the first 7 receivers, closest to the fault trace and the first receiver at the fault top, is $0.166W$, while that of the following 7 is $0.333W$, defining a propagation distance of about $3.3W$ along the receiver lines.

Fig. 7 shows unfiltered velocity and displacement fault-parallel synthetic seismograms for F1–F3 along L2 obtained from the spontaneous rupture propagations. In agreement with previous studies on supershear earthquakes (e.g. Dunham and Bhat, 2008), the most distinctive feature in the synthetic seismograms is the two energy 'packages', separated by an increasing time-window as the propagation distance r increases (Fig. 7). The amplitude-decay of the fastest-travelling package is much faster than that for the package with slower speed. As explained by Dunham and Archuleta (2005), the fastest-travelling package consists mainly of evanescent P-waves with amplitudes decreasing exponentially with distance and frequency. The more slowly-propagating package corresponds to the wavefield generated by superposition of shear and Rayleigh Mach waves (see Dunham and Bhat, 2008). While the planar Rayleigh Mach wave does not experience any attenuation in a homogeneous elastic halfspace, the shear Mach wave attenuates because of two geometrical factors: the finiteness of the fault width and the shape of the supershear rupture front. These factors determine how the seismic energy carried by the S-wave spreads spatially. Assuming a linear rupture front the shear Mach wave becomes cylindrical with amplitude decrease as the inverse square-root of r for distances much larger than W (i.e. $r \gg W$). For real earthquakes, the two energy 'packages' are not expected to be clearly identified separately in observed records. The presence of noise and rupture complexity may cause this to happen. Moreover, intrinsic bulk dissipation (i.e. the quality factor Q) and intrinsic scattering contribute to the dispersion and attenuation rate of the Mach wavefield as well. None of these effects are included in Fig. 7.

Fig. 8 shows the average D_c'' values estimated from Mach waves generated by model F2 and recorded along receiver lines L1, L2 and L3 by the method proposed by Cruz-Atienza et al. (2009), i.e., using the displacement at the time of the peak strike-parallel particle velocity (dashed line). Clearly, the method does not provide reliable estimates of D_c at any distance from the fault (note that the prescribed D_c value in this simulation is 0.8 m). An approximation of the slip and slip-rate functions far more accurate than that provided by the off-fault synthetic seismograms is clearly needed in order to obtain reasonable estimates of the breakdown slip from Mach waves.

4.2. Slip and slip-rate asymptotic approximation

Let us concentrate on the Mach wavefield sufficiently far from the fault for the integrated contributions of the near-field, the P- and S-wave intermediate-fields, the P-wave far-field, and the stopping

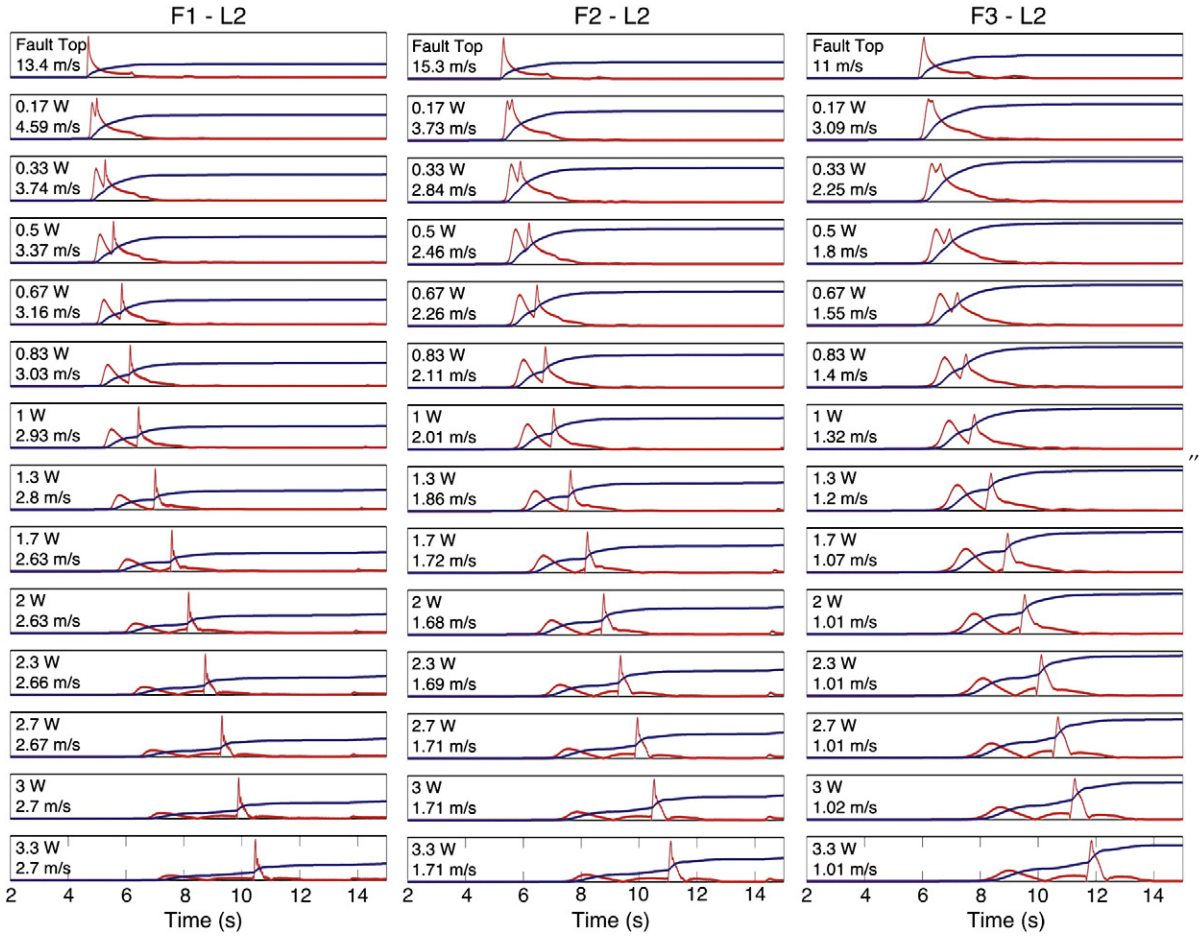

Fig. 7. Rake-parallel (black, or red in the electronic version of this article) particle velocity and (gray, or blue in the electronic version of this article) displacement synthetics for rupture cases F1–F3 along receiver line L2 (see Fig. 6). The values in the left side of the panels list the distance along the receiver line measured from the fault (in units of W), as well as the peak velocity.

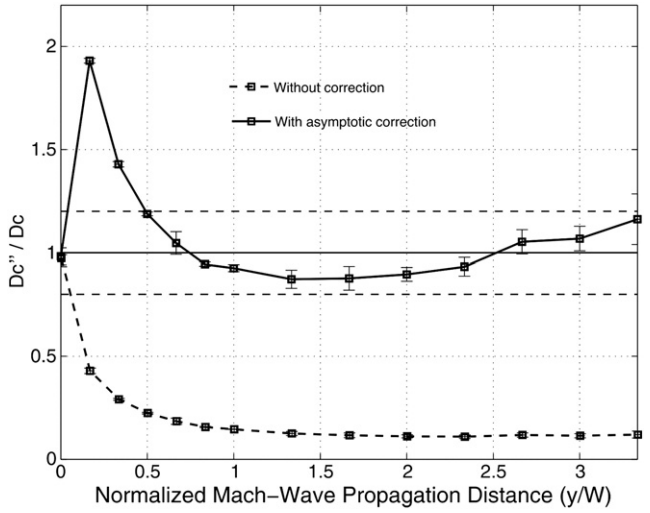

Fig. 8. Average ratio of D_c'' and D_c estimated from Mach waves recorded along receiver lines L1, L2 and L3 (see Fig. 6) as (dashed line) the displacement at the time of the peak strike-parallel particle velocity, and as (solid line) the slip at the time of the peak slip-rate estimated from the synthetic displacements and particle velocity using Eq. (2).

phases to be negligible. We will thus consider a model including a free-surface region where a simple asymptotic approximation is sufficient to accurately describe the synthetic seismograms. For kinematic source models, Bernard and Baumont (2005) derived an asymptotic approximation for S-wave fault-parallel displacements in the far-field of a full-space, produced by supershear ruptures:

$$u_p^{II}(t,r) \approx \left[u_A^{II}(t)\right] \cdot \frac{\cos 2\theta}{2\sin(\theta)} \cdot H(t - r/v_s) \cdot \left(1 + \frac{r}{r_0}\cos(\theta)\right)^{-1/2}. \quad (1)$$

This Mach wave representation formula has three main features (see Fig. 6): 1) fault parallel displacements at a given point P, u_P^{II}, are proportional to the slip function in the vicinity of the critical point A, $[u_A^{II}]$, with a time shift equal to the S-wave arrival time; 2) displacements are modulated by a radiation pattern depending on the take-off angle θ; and 3) the amplitude of the displacements decreases as the inverse square-root of the propagation distance, r. The parameter r_0 describes the rupture front curvature. The time derivative of Eq. (1) reveals that the fault-parallel velocity field at P is proportional to the slip-rate function at A. Thus, the slip and slip-rate functions at point A can be approximated by the product of the recorded Mach wavefield at P and a function of several parameters, $f(r,\theta,r_0)$, as:

$$\begin{aligned} \left[u_A^{II}(t)\right] &\approx u_P^{II}(t,r) \cdot f(r,\theta,r_0) \\ \left[\dot{u}_A^{II}(t)\right] &\approx \dot{u}_P^{II}(t,r) \cdot f(r,\theta,r_0) \end{aligned} \quad (2)$$

for $t \geq r/v_s$. Notice, however, that Eq. (1) does not consider the effect of the free surface (FS), which amplifies the ground motion and induces the generation of Rayleigh Mach waves when rupture reaches the Earth's surface (Dunham and Bhat, 2008). Therefore, to account for the effect due to the FS, we introduce a tuning factor α_{fs} in Eq. (2) so that the function f is given by:

$$f(r) = \frac{2\alpha_{fs}\sin(\theta)}{\cos(2\theta)} \cdot \sqrt{1 + \frac{r}{r_0}\cos(\theta)}. \quad (3)$$

Eq. (2) can now be used to approximate slip and slip-rate functions at the critical points A from displacement and velocity seismograms along receiver lines L1, L2 and L3. We thus define D_c'' for supershear ruptures as the value of the slip function at the time of the peak slip-rate approximated by Eq. (2). However, for real earthquakes, the most difficult parameter to estimate is probably r_0, the radius of curvature for the rupture front. For this reason, we performed a grid search over a wide range of values for r_0 to minimize the relative least-square misfit between D_c' values determined from slip and slip-rate functions at point A, and D_c'' values as defined above by means of Eq. (2) (i.e. by estimating slip and slip-rate time histories at points A from recorded seismograms). Fig. 9 shows, for each rupture scenario, the least-square error as a function of r_0 normalized by W along the L2 receiver line. Each error line corresponds to one of 13 different off-fault receivers. Lines with the highest misfit for any value of r_0 correspond to receivers close to the fault trace (within ~0.5W), where the far-field asymptotic solution is not sufficiently accurate to approximate the recorded wavefield. The error minimization procedure reveals decreasing curvature radii, r_0, for which most of the error curves are at a minimum for F1 (~2W), F2 (~0.33W) and F3 (~0.2W). This result is in agreement with the rupture-time contours in Fig. 2, where the rupture front curvature increases with D_c. From these findings, we suggest an average value of r_0 of about 1W to be used for practical purposes, when other details of the rupture geometry are unconstrained. By trial and error modelling we estimate an optimum FS correction factor α_{fs} of about 1.5.

Fig. 10 shows a comparison between the slip-rate functions at the critical point A (red lines) with those estimated throughout Eq. (2)

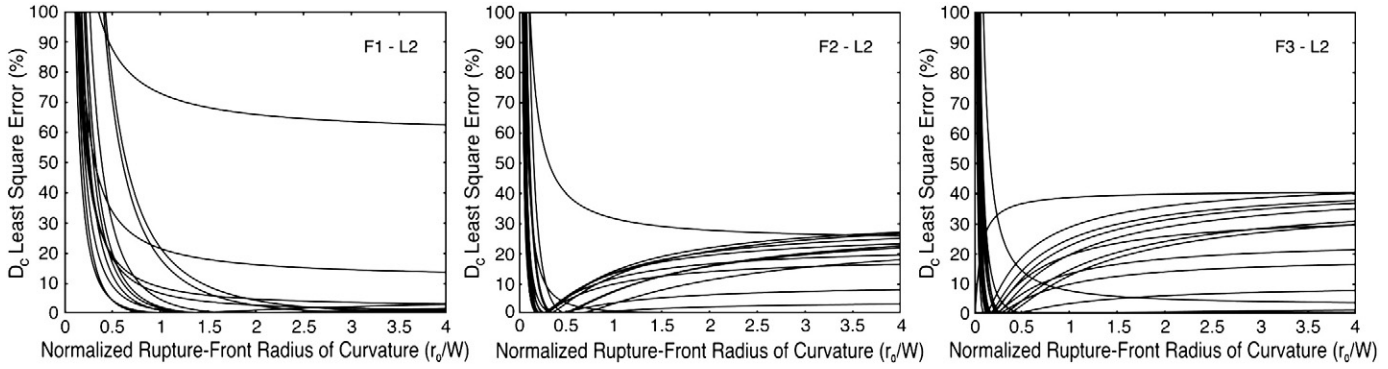

Fig. 9. Least-square error as a function of r_0 normalized by W along the L2 receiver line (see Fig. 6) for rupture scenarios F1 (left), F2 (center), and F3 (right) (see text for details on location). Each line corresponds to one of 13 different off-fault receivers.

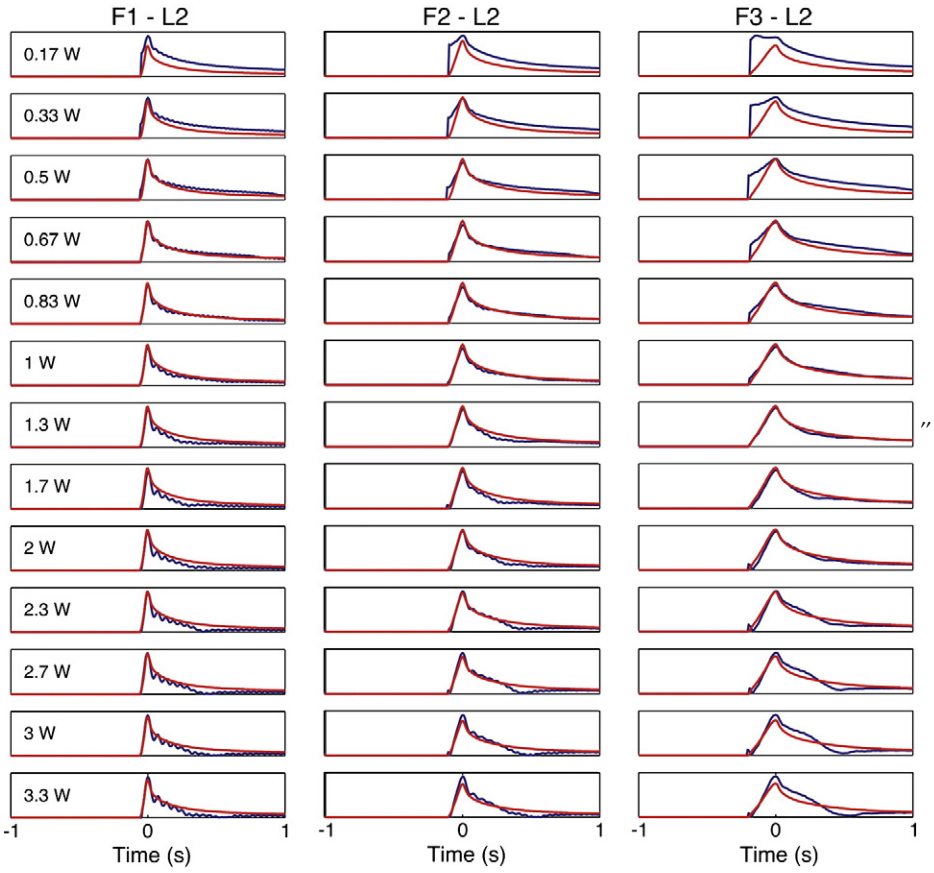

Fig. 10. Comparison between the slip-rate functions at the critical point A for receivers along the L2 receiver line (black signals, or red signals in the electronic version of this article) with those estimated from Eq. (2) (gray signals, or blue signals in the electronic version of this article). The peak values of the signals are centered at the origin time.

using the spontaneous-rupture rake-parallel synthetic seismograms along L2 for all rupture scenarios (blue lines). Fits obtained along receiver lines L1 and L3 are comparable (not shown). The on-fault slip-rate functions show significant discrepancies to the corrected seismograms from the spontaneous rupture models at the stations located less than ~0.5W from the fault. However, beyond these stations and up to a distance of more than three times the fault width the reconstruction of the on-fault slip-rate functions from the Mach wavefield seismograms is remarkably accurate, in particular for the F2 case, where $D_c = 0.8$ m. In fact, D_c is estimated within an accuracy of 20% using corrected synthetic seismograms at distances between 0.5W and 3.5W from the fault (see solid line, Fig. 8).

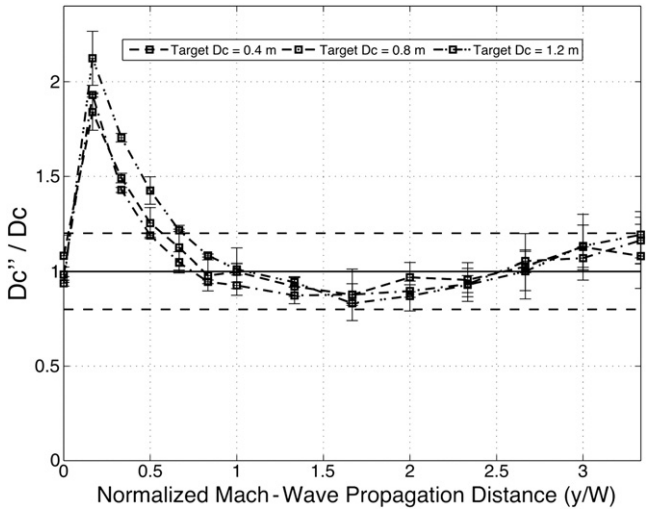

Fig. 11. Average ratios of D_c''/D_c along receiver lines L1, L2 and L3 for cases F1–F3. The error bars depict the mean ± 1 standard deviation, and the dashed lines represent deviations of 20% from a perfect fit between D_c'' and D_c.

4.3. Breakdown slip estimated from off-fault Mach-wave records

In this section we assess the resolution of D_c'' measurements to be used as a proxy for D_c. The resolution tests are carried out in elastic and visco-elastic halfspace models. First, we revisit scenarios F1 (D_c = 0.4 m), F2 ($D_c = 0.8$ m) and F3 ($D_c = 1.2$ m), discussed in an earlier section (see Fig. 10 for a comparison of the slip-rate function at the critical point A with the corrected fault-parallel seismograms along L2 for each scenario). From the seismograms along L1, L2 and L3 we compute average D_c'' values as a function of the Mach wave propagation distance (Fig. 11). D_c'' is found to be within the 20% of the prescribed D_c on the fault for distances to the fault trace larger than 0.5W (i.e. >~3 km), except for F3 (discrepancies up to 40%). At distances smaller than 3 km, estimates increase rapidly reaching values with a deviation of about 90% at distances of 0.33W (i.e. 1 km) from the fault.

Fig. 12 presents results for a model with lower seismic velocities ($v_s = 2000$ m/s, $v_p = 3460$ m/s) and density ($\rho = 1880$ kg/cm^3) as compared to those in Fig. 11, and traction and friction parameters as for F2. The first scenario (D1) is carried out in a loss-less (i.e. elastic) model, while the second scenario (D2) includes intrinsic attenuation ($Q_s = 100$ and $Q_p = 9/4 * Q_s = 225$). Despite the energy loss with propagation distance for D2 as compared to D1, the D_c'' estimates for both scenarios are within 40% of the prescribed D_c. Moreover, this

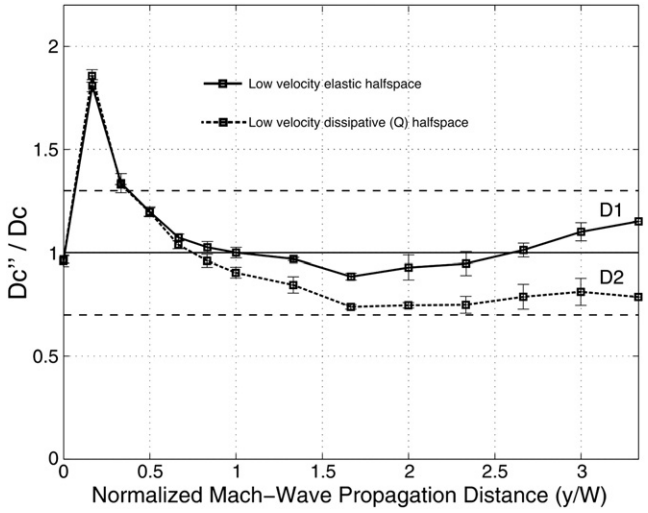

Fig. 12. Comparison of D_c''/D_c ratios for two simulations D1 and D2 in a half-space model with $v_s = 2000$ m/s, $v_p = 3460$ m/s and $\rho = 1880$ kg/cm^3, and traction and friction parameters as for F2. D1 is carried out in a loss-less model, while D2 includes intrinsic attenuation ($Q_s = 100$ and $Q_p = 225$). The dashed lines depict D_c'' deviations of 40% from the prescribed D_c.

exercise also shows that our Mach-wave asymptotic correction is independent of the elastic properties of the medium, at least for the models tested here.

5. Estimation of Dc from strong-motion records of historical earthquakes

In this section we estimate D_c on fault segments of historical earthquakes where there is strong evidence that rupture has propagated with supershear speeds. We analyze two such events, namely the 2002 M_w7.9 Denali, Alaska, and the 1999 M_w7.6 Izmit, Turkey, earthquakes. These events have high-quality strong-motion records available in the distance range from the fault for which our method is valid (about 3 km to more than 16 km).

5.1. The 2002 M_w7.9 Denali earthquake

The 2002 Denali earthquake ruptured a total of 340 km on three different faults. The earthquake initiated as a thrust fault on the 40-km-long Susitna Glacier fault before jumping onto the nearly vertical

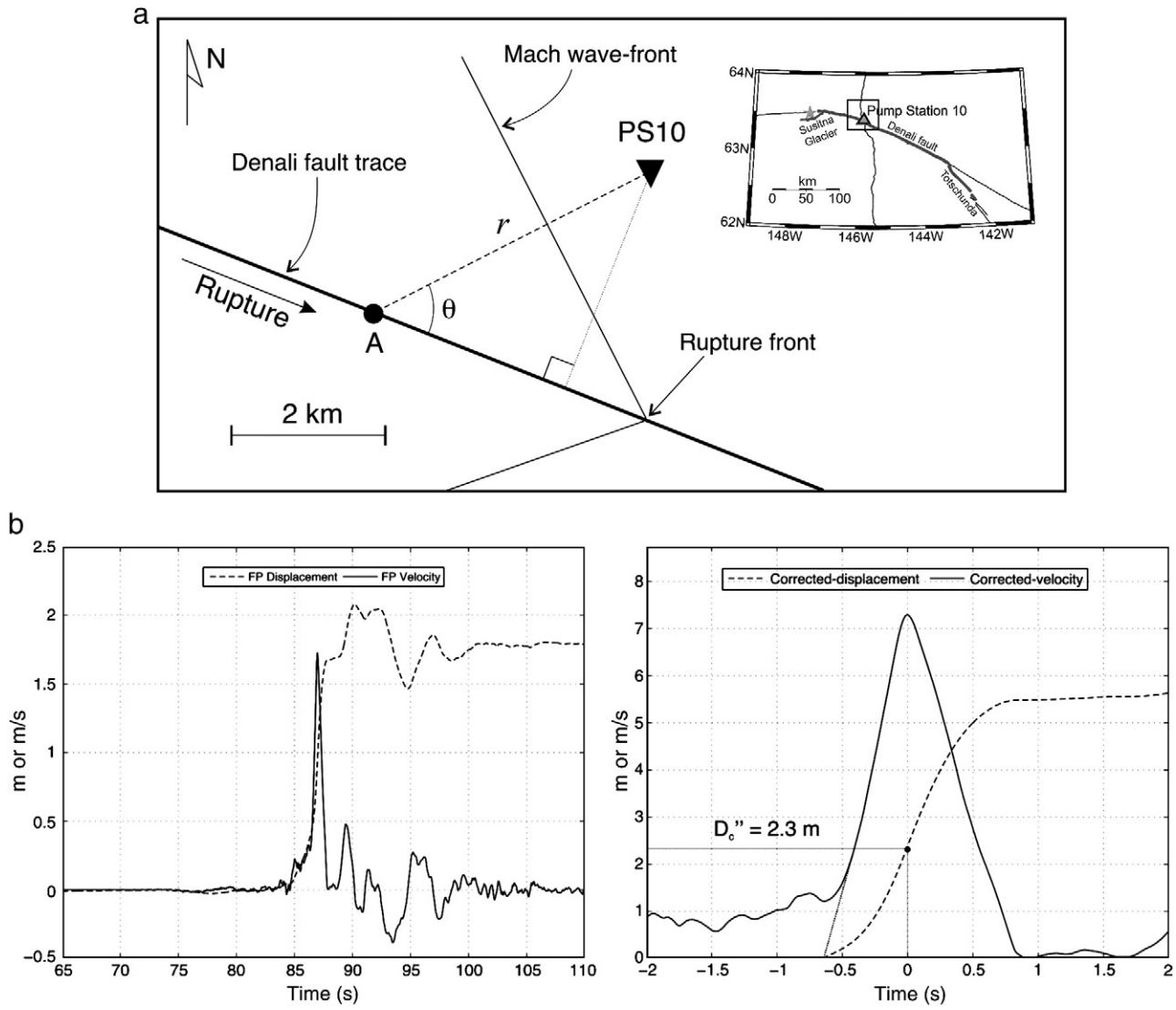

Fig. 13. D_c'' estimate for the 2002 Denali earthquake. (a) Illustration of Mach wave propagation from the fault to station PS10 within the area depicted by the small rectangle in the map shown in the upper right corner. (b) (left) Fault parallel (FP) particle velocity and displacement recorded at PS10 (Ellsworth et al., 2004). (b) (right) Slip and slip-rate time series estimated from the PS10 record FP particle velocity and displacement records. The displacement ahead of the Mach wave has been removed.

Denali fault. After propagating 240 km eastward on the right-lateral Denali fault, the rupture continued another 70 km southeastward on the Totschunda fault and stopped. The seismograms of interest for our purpose obtained from this earthquake are those recorded at Pump Station10 (PS10), located 3 km north of the fault trace (see Fig. 13a). Finite fault inversions (Eberhart-Phillips et al., 2003; Oglesby et al., 2004) support a right-lateral strike-slip mechanism on the approximately vertical Denali fault, with about 5–6 m of nearly horizontal slip near PS10. The PS10 records were carefully corrected and calibrated by Ellsworth et al. (2004) and Evans et al. (2006). Several studies argue in favor of rupture propagating at supershear velocities along the Denali fault segment near PS10 (Ellsworth et al., 2004; Aagaard and Heaton, 2004; Dunham and Archuleta, 2004; Aagaard et al., 2004; Dunham and Archuleta, 2005). Evidence of supershear propagation in the PS10 records include a larger peak velocity on the fault-parallel (FP) as compared to the fault-normal (FN) component, as well as several later-arriving pulses on the FN component.

Fig. 13b (left) shows both FP velocity and displacement records, and the propagation parameters for the Mach wave arriving at PS10. Following Dunham and Archuleta (2004) we interpret the first and more prominent arrival of the FP velocity component as the Mach wave generated by supershear stress release. Furthermore, we assume that the Mach wave primarily originates from rupture propagation on the Denali fault in close vicinity of PS10 (critical point A, Fig. 13a). Ellsworth et al. (2004) estimated the rupture speed on the fault segment near PS10 to be about 5.3 km/s at a depth of about 5 km, where the S-wave speed (average for the upper 10 km) is about 3.2 km/s. Thus, the critical angle for the Mach waves recorded at PS10, located approximately 3 km from the fault, is about $\arccos(3.2/5.3) = 53^\circ$ with a propagation distance of 3.8 km. If we apply these values in Eq. (2), along with $r_0 \sim 1W \sim 12$ km (e.g., Oglesby et al., 2004), and eliminate the displacement accumulated ahead of the Mach wave arrival (as we did for the synthetic seismograms in Fig. 10), which is presumably due to near-field effects, we obtain the slip and slip-rate time histories shown in Fig. 13b (right), which produce a D_c'' value of about 2.3 m. Notice that such procedure, which produces an estimate of the breakdown slip D_c at A, is in agreement with the final slip of 5–6 m found independently by other investigators on that fault segment (see Ellsworth et al., 2004).

5.2. The 1999 M_w7.6 Izmit, Turkey, earthquake

The 1999 Izmit earthquake ruptured bi-laterally almost 150 km of the westernmost section of the North Anatolian fault with

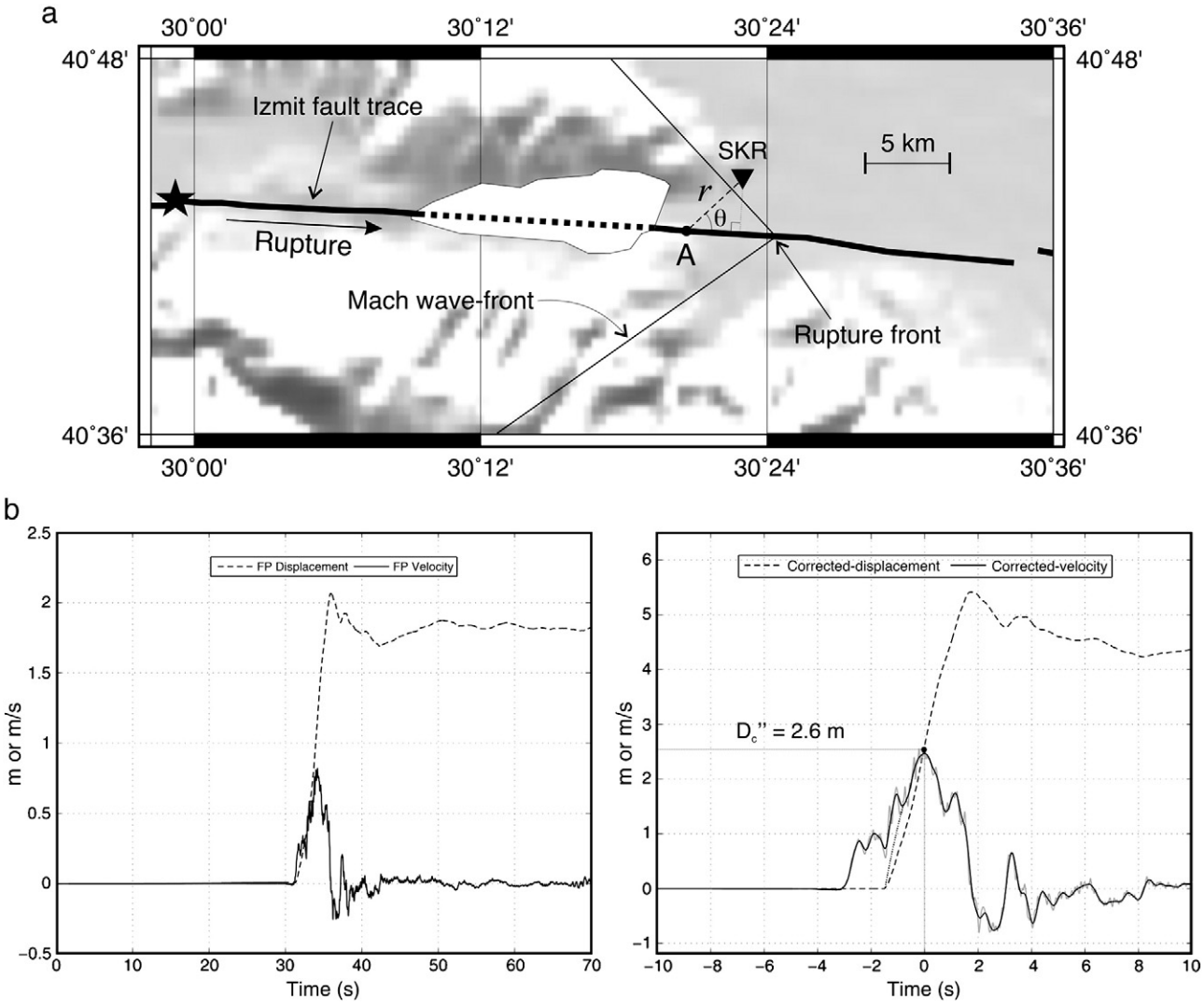

Fig. 14. D_c'' estimate for the 1999 Izmit earthquake. (a) Illustration of Mach wave propagation from the fault to station SKR. (b) (left) Fault parallel (FP) particle velocity and displacement recorded at SKR (Bouchon et al., 2001). (b) (right) Slip and slip-rate time series estimated from the SKR records of FP particle velocity and displacement records. The displacement ahead of the Mach wave has been removed.

predominantly right-lateral motion, on a near vertical, east–west trending part of the fault extending to a depth of about 20 km (Toksöz et al., 1999; Özalaybey et al., 2002). Different studies provide strong arguments in favor of rupture propagating faster than the shear wave velocity along the 50 km-long Izmit–Sapanca Lake–Sakarya fault segment (Ellsworth and Celebi, 2000; Bouchon et al., 2000; Bouchon et al., 2002), primarily based on two observations: 1) the asymmetry of the rupture-time isochrones with respect to the epicenter revealed by kinematic source imaging, from which the rupture front appears to break the whole segment in only 10 s and, 2) the S–P arrival time difference at the strong motion station SKR, located 2.8 km away the fault trace (Fig. 14a), is remarkably short (Bouchon et al., 2002). For these reasons, and in agreement with Bouchon et al. (2002), we assume that the most prominent early pulses recorded at SKR correspond to the Mach wave excited by the supershear rupture transient, as sketched in Fig. 14a.

Fig. 14b (left) shows FP unfiltered velocity and displacement records at station SKR. The rupture speed near SKR is estimated at about 4.8–4.9 km/s (Bouchon et al., 2002). Assuming that the Mach wave at SKR is generated on the fault in close vicinity of the station, we estimate a representative S-wave speed of 2.8 km/s from Mooney et al. (1998) as an average of the upper 10 km crust. Thus, the critical angle for the Mach waves recorded at SKR located about 2.8 km from the fault is about $\arccos(2.8/4.9) = 55°$ with a propagation distance of 3.4 km. Using Eq. (2), along with $r_0 \sim 1W \sim 16$ km (Bouchon et al., 2002), and eliminating the displacement accumulated ahead of the Mach wave arrival as done for the Denali earthquake we obtain a D_c'' value of about 2.6 m from the slip and slip-rate time histories shown in Fig. 14b (right). In order to better identify the Mach wave arrival time we low-pass filtered the corrected velocity field with a 2.0 Hz corner frequency (black line). It is remarkable that our approximation of the slip history at the critical point A of the supershear fault segment (obtained for our D_c'' estimate) is in agreement with the final slip of 4–5 m obtained independently by Bouchon et al. (2002) through a source-imaging inversion procedure for the 1999 Izmit earthquake.

6. Discussion and conclusions

We present a new method to estimate the breakdown slip (D_c) using Mach waves recorded from rupture propagation with supershear speeds. The method uses the approach by Mikumo et al. (2003), where D_c is estimated as the slip at the time of the peak slip rate for subshear rupture propagation. We first validate the technique by Mikumo et al. for supershear rupture propagation and then apply the method to estimate D_c from an asymptotic approximation of the strike-parallel slip and slip-rate from Mach waves identified in strong-motion records. The method is tested using spontaneous-rupture simulations with supershear rupture speeds. Our results show that D_c can be estimated within an error of 40% from Mach waves that have propagated at least 3 km from the fault (about 2.8 km perpendicular from the fault). For the simple visco-elastic half-space models tested here, this accuracy is maintained out to distances of at least 20 km of Mach wave propagation (about 16 km perpendicular to the fault). We apply the method to estimate D_c from Mach waves recorded for the 2002 M_w7.9 Denali, Alaska, earthquake (~2.3 m, station PS10) and for the 1999 M_w7.6 Izmit, Turkey, earthquake (~2.6 m, station SKR). However, these values may be overestimating D_c since both stations are very close to the fault, where the far-field asymptotic approach may be less accurate. Considering a maximum deviation of D_c'' from D_c (~50% overprediction) at a distance of 3 km from the fault obtained in our numerical results shown in Fig. 11 (i.e. at a distance of $0.5W$), more accurate values of D_c within the supershear fault segments of the Denali and Izmit events would be 1.5 m and 1.7 m, respectively.

Dunham and Bhat (2008) found a characteristic distance, comparable to the fault width W, where two asymptotic solutions describing the Mach wavefield coincide. For distances to the fault smaller than about W, they concluded that the sub-surface wavefield excited by supershear ruptures is accurately predicted by an along-dip unbounded slip zone radiating seismic waves with amplitudes undiminished with r. For distances beyond W, they claim that rupture can be modelled satisfactorily as a moving point-source producing shear- and Rayleigh-wave Mach fronts with amplitudes (at least those of the shear Mach wave) decreasing as the inverse square-root of the fault-perpendicular distance. In the following we have designed four rupture scenarios with different W to test whether or not the fault width is a characteristic length determining the distance from the fault beyond which our asymptotic approximation accurately predicts the Mach wavefield.

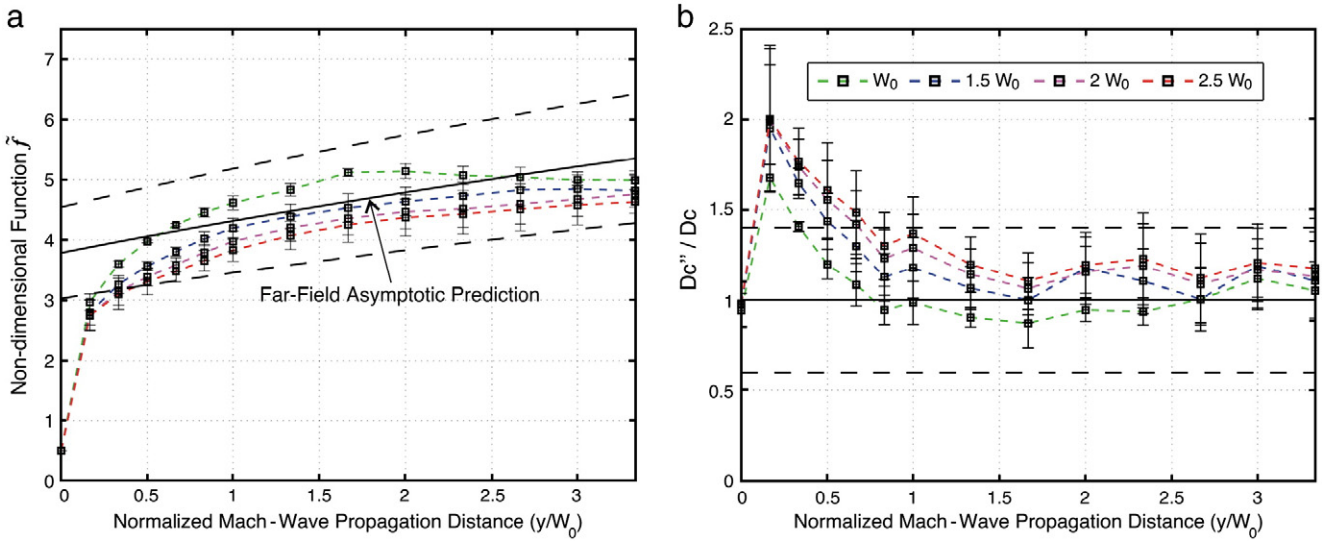

Fig. 15. (a) Comparison of the analytical function f for the asymptotic representation (Eq. (3), solid black line) to function $\tilde{f}$. The dashed right lines depict $\tilde{f} \pm 20\%$ error. f is estimated using the mean take-off angle θ for the four rupture scenarios (53.19°). Functions $\tilde{f}$ computed from Eq. (4) for each of the rupture scenarios are shown for fault widths of W_0, $1.5W_0$, $2W_0$ and $2.5W_0$ with $W_0 = 6$ km. (b) Ratios of D_c''/D_c for the curves in (a), where the dashed right lines depict deviations of 40% from a perfect fit between D_c'' and D_c.

For this purpose, we define function $\tilde{f}$ as the ratio of the peak slip-rate at A and the peak particle velocity at P using Eq. (2):

$$\tilde{f}(r) \approx \frac{\max\left\{\left[\dot{u}_A^{II}\right]\right\}}{\max\left\{\dot{u}_P^{II}(r)\right\}}, \tag{4}$$

at a distance r from the fault. $\tilde{f}$ provides a first check on how close the off-fault particle velocity is to the slip-rate, by comparing the peak values only. However, the most interesting property of this function is the possibility of assessing how much the amplitude of the far-field asymptotic approximation given by Eq. (1) deviates from that of the complete elastodynamic solution. Since $\tilde{f}$ is generated from the numerically-computed functions $[\dot{u}_A^{II}]$ and $\dot{u}_P^{II}(r)$, the comparison of $\tilde{f}$ with the analytical function f (as defined in Eq. (3)) for different fault widths would to some extent reveal the influence of W on discrepancies between D_c'' and D_c. We thus compute the function $\tilde{f}$ from velocity seismograms along the receiver lines L1, L2 and L3 and their corresponding slip-rate functions at points A, and compare to f for 4 different fault widths W (case K1: $W=W_0$; case K2: $W=1.5W_0$; case K3: $W=2W_0$; and case K4: $W=2.5W_0$, where $W_0=6$ km) at increasing distance from the fault (Fig. 15a). Here, the calculations of f used average values for θ and r_0 (fault width) from the K1–K4 scenarios. All scenarios have the same initial traction conditions and D_c as those defined for case F1. The estimates based on the spontaneous-rupture simulations, which consider the complete wavefield solution, are all within 20% of the asymptotic prediction (black dashed lines) for distances from the fault further than $0.5W_0$. Notice that the $\tilde{f}$ estimates for all cases do not deviate by more than 20% from f for much less than the corresponding fault width for all rupture cases, as would be expected if W determined the minimum distance from the fault for which the asymptotic representation accurately describes the amplitude of seismograms. This observation suggests that the approach we have introduced to estimate slip and slip-rate functions from Mach waves should also be essentially insensitive to the fault width. To confirm this, Fig. 15b shows D_c''/D_c ratios for cases K1–K4 computed using our definition of D_c'' that involves Eq. (2). As expected, the prescribed D_c on the fault (0.4 m) is approximated within 50% of the target by D_c'' for all cases and distances (along the Mach wave propagation paths) greater than about $0.66W_0$ (i.e., $r>4.0$ km), which implies fault-perpendicular distances greater than about 3 km. Since PS10 and SKR are located about that distance from the corresponding fault traces, these results support that $D_c'' \sim 1.5D_c$ for both events, as argued above from Fig. 11.

The numerical tests supporting our proposed method for estimating D_c from Mach waves were conducted in simple visco-elastic half-spaces. It is possible that the accuracy of the method is degraded for Mach waves propagating in more realistic crustal structure (i.e., fault gouge, near-surface low-velocity layers, sedimentary basins etc.) However, it is beyond this study to explore the wide range of effects that such features may have on Mach waves. This problem is left for work specific to near-fault Mach waves recorded during future strike-slip events within a known, complex crustal structure.

Acknowledgements

We thank M. Bouchon for his constructive view of this work and for providing seismic records of the 1999 Izmit event (Fig. 15b, left) as well as the fault map included in Fig. 15a. We thank J. Evans and W. Ellsworth for providing us the corrected seismic records of the 2002 Denali earthquake at the PS10 station (Fig. 14b, left). We finally thank E. Dunham, J. Virieux and P. Bernard for their enlightening comments. The numerical simulations in this study were carried out on Pohualli, a parallel-computing cluster sponsored by CONACyT through project number 80205. This research was supported by UNAM through the PAPIIT project number IN119409 and by the Southern California Earthquake Center (SCEC). SCEC is funded by NSF Cooperative Agreement EAR-0529922 and USGS Cooperative Agreement 07HQAG0008. The SCEC contribution Number for this paper is 1429.

References

Aagaard, B.T., Heaton, T.H., 2004. Near-source ground motions from simulations of sustained intersonic and supersonic fault ruptures. Bull. Seismol. Soc. Am. 94 (6), 2064–2078.

Aagaard, B., Anderson, G., Hudnut, K.W., 2004. Dynamic rupture modeling of the transition to strike-slip motion in the 2002 Denali fault, Alaska, earthquake. Bull. Seismol. Soc. Am. 94 (no. 6B), S190–S201.

Andrews, D.J., 1976. Rupture velocity of plane-strain shear cracks. J. Geophys. Res. 81, 5679–5687.

Bernard, P., Baumont, D., 2005. Shear Mach wave characterization for kinematic rupture models with constant supershear rupture velocity. Geophys. J. Int. 162, 431–447.

Bizzarri, A., Spudich, P., 2008. Effects of supershear rupture speed on the high-frequency content of S waves investigated using spontaneous dynamic rupture models and isochrone theory. J. Geophys. Res. 113, B05304. doi:10.1029/2007JB005146.

Bizzarri, A., E.M. Dunham, and P. Spudich (2009). Coherence of Mach fronts during heterogeneous supershear earthquake rupture propagation: simulations and comparison with observations, J. Geophys. Res., submitted for publication 24 July.

Bouchon, M., Valée, M., 2003. Observation of Long Supershear Rupture During the Magnitude 8.1 Kunlunshan Earthquake. Science 301, 824–826.

Bouchon, M., Karabulut, H., 2008. The aftershock signature of supershear earthquakes. Science 320, 1323–1325. doi:10.1126/science.1155030.

Bouchon, M., Toksoz, N., Karabulut, H., Bouin, M.P., Dietrich, M., Aktar, M., Edie, M., 2000. Seismic imaging of the 1999 Izmit (Turkey) rupture inferred from the near-fault recordings. Geophys. Res. Lett. 27, 3013–3016.

Bouchon, M., Bouin, M., Karabulut, H., Toksöz, M.N., Dietrich, M., Rosakis, A.J., 2001. How fast is rupture during an earthquake? New insights from the 1999 Turkey Earthquakes. Geophys. Res. Lett. 28 (14), 2723–2726.

Bouchon, M., Nafi Toks0z, M., Karabulut, H., Bouin, M.-P., Dietrich, M., Aktar, M., Edie, M., 2002. Space and time evolution of rupture and faulting during the 1999 Izmit (Turkey) earthquake. Bull. Seismol. Soc. Am. 92, 256–266.

Burridge, R., 1973. Admissible speeds for plane-strain self-similar shear cracks with friction but lacking cohesion. Geophys. J. 35, 439–455.

Cruz-Atienza, V.M., Virieux, J., 2004. Dynamic rupture simulation of non-planar faults with a finite-difference approach. Geophys. J. Int. 158, 939–954.

Cruz-Atienza, V.M., Virieux, J., Aochi, H., 2007. 3D finite-difference dynamic-rupture modelling along non-planar faults. Geophysics 72 (SM123). doi:10.1190/1.2766756.

Cruz-Atienza, V.M., Olsen, K.B., Dalguer, L.A., 2009. Estimation of the breakdown slip from strong-motion seismograms: insights from numerical experiments. Bull. Seismol. Soc. Am. 9, 3454–3469. doi:10.1785/0120080330.

Dalguer, L.A., Day, S., 2007. Staggered-grid split-node method for spontaneous rupture simulation. J. Geophys. Res. 112, B02302. doi:10.1029/2006JB004467.

Das, S., 2007. The need to study speed. Science 317, 905–906. doi:10.1126/science.1142143.

Das, S., Aki, K., 1977. A numerical study of two-dimensional spontaneous rupture propagation. Geophys. J. R. Astron. Soc. 50, 643–668.

Day, S.M., 1982. Three-dimensional simulation of spontaneous rupture: the effect of nonuniform prestress. Bull. Seismol. Soc. Am. 72, 1881–1902.

Dunham, E., Bhat, H.S., 2008. Attenuation of radiated ground motion and stresses from three-dimensional supershear ruptures. J. Geophys. Res. 113, B08319. doi:10.1029/2007JB005182.

Dunham, E.M., Archuleta, R.J., 2004. Evidence for a supershear transient during the 2002 Denali Fault earthquake. Bull. Seismol. Soc. Am. 94 (6B), S256–S268. doi:10.1785/0120040616.

Dunham, E.M., Archuleta, R.J., 2005. Near-source ground motion from steady state dynamic rupture pulses. Geophys. Res. Lett. 32 (L03302). doi:10.1029/2004 GL021793.

Eberhart-Phillips, D., et al., 2003. The 2002 Denali fault earthquake, Alaska: a large-magnitude, slip-partitioned event. Science 300, 1113–1118.

Ellsworth, W.L., Celebi, M., 2000. Near field displacement time histories of the M 7.4 Kocaeli (Izmit), Turkey, earthquake of August 17, 1999. Am. Geophys. Union Fall Meet. Suppl. vol. 80, F648.

Ellsworth, W.L., Celebi, M., Evans, J.R., Jensen, E.G., Metz, M.C., Nyman, D.J., Roddick, J.W., Spudich, P., Stephens, C.D., 2004. Near-field ground motions of the M 7.9 November 3, 2002, Denali fault, Alaska, earthquake recorded at pump station 10. Earthq. Spectra 20, 597–615.

Evans, J.R., Jensen, E.G., Sell, R., Stephens, C.D., Nyman, D.J., Hamilton, R.C., Hager, W.C., 2006. Calibration of PS09, PS10, and PS11 Trans-Alaska pipeline system strong-motion instruments, with acceleration, velocity, and displacement records of the Denali Fault earthquake, 03 November 2002. Open-File Report 2006–1028, U.S. Department of the Interior and U.S. Geological Survey.

Freund, L.B., 1998. Dynamic Fracture Mechanics. Cambridge University Press.

Fukuyama, E., Mikumo, T., 2007. Slip-weakening distance estimated at near-fault stations. Geophys. Res. Lett. 34. doi:10.1029/2006GL029203.

Fukuyama, E., Mikumo, T., Olsen, K.B., 2003. Estimation of the critical slip-weakening distance: theoretical background. Bull. Seismol. Soc. Am. 93, 1835–1840.

Gottschaemmer, E., Olsen, K.B., 2001. Accuracy of the explicit planar free-surface boundary condition implemented in a fourth-order staggered-grid velocity–stress finite-difference scheme. Bull. Seismol. Soc. Am. 91, 617–623.

Guatteri, M., Spudich, P., 2000. What can strong motion data tell us about slip-weakening fault friction laws? Bull. Seismol. Soc. Am. 90, 98–116.
Ida, Y., 1972. Cohesive force across the tip of a longitudinal-shear crack and Griffith's specific surface energy. J. Geophys. Res. 77, 3796–3805.
Ide, S., Takeo, M., 1997. Determination of constitutive relations of fault slip based on seismic waves analysis. J. Geophys. Res. 102 (27), 379–27,391.
Madariaga, R., Olsen, K.B., Archuleta, R., 1998. Modeling dynamic rupture in a 3D earthquake fault model. Bull. Seismol. Soc. Am. 88, 1182–1197.
Marcinkovich, C., Olsen, K., 2003. On the implementation of perfectly matched layers in a three-dimensional fourth-order velocity–stress finite difference scheme. J. Geophys. Res. 108 (no. B5), 2276. doi:10.1029/2002JB002235.
Matsu'ura, M., Kataoka, H., Shibazaki, B., 1992. Slip-dependent friction law and nucleation processes in earthquake rupture. Tectonophysics 211, 135–148.
Mikumo, T., Yagi, Y., 2003. Slip-weakening distance in dynamic rupture of in-slab normal-faulting earthquakes. Geophys. J. Int. 155, 443–455.
Mikumo, T., Olsen, K.B., Fukuyama, E., Yagi, Y., 2003. Stress-breakdown time and critical weakening slip inferred from the source time functions on earthquake faults. Bull. Seismol. Soc. Am. 93, 264–282.
Mooney, W.D., Laske, G., Masters, G., 1998. CRUST 5.1: a global crustal model at 5°×5°. J. Geophys. Res. 103, 727–747.
Oglesby, D.D., Dreger, D.S., Harris, R.A., Ratchkovski, N., Hansen, R., 2004. Inverse kinematic and forward dynamic models of the 2002 Denali, Alaska earthquake. Bull. Seismol. Soc. Am. 94 (B6), S214–S233.
Ohnaka, M., Yamashita, T., 1989. A cohesive fault model for dynamic shear faulting based on experimentally inferred constitutive relation and strong motion source parameters. J. Geophys. Res. 94, 4089–4104.
Ohnaka, M., Kuwahara, Y., Yamamoto, K., 1987. Constitutive relations between dynamic physical parameters near a tip of the propagating slip zone during stick-slip shear failure. Tectonophysics 144, 109–125.
Olsen, K.B., Madariaga, R., Archuleta, R.J., 1997. Three-dimensional dynamic simulation of the 1992 Landers earthquake. Science 278, 834–838.
Olsen, K.B., Day, S.M., Minster, J.B., Cui, Y., Chourasia, A., Okaya, D., Maechling, P., Jordan, T., 2008. TeraShake2: Spontaneous rupture simulations of Mw 7.7 earthquakes on the southern San Andreas fault. Bull. Seismol. Soc. Am. 98 (no. 3), 1162–1185. doi:10.1785/0120070148.
Özalaybey, S., Ergin, M., Aktar, M., Tapirdamaz, C., Biçmen, F., Yörük, A., 2002. The 1999 Izmit Earthquake Sequence in Turkey: Seismological and Tectonic Aspects. Bull. Seismol. Soc. Am. 92 (1), 376–386. doi:10.1785/0120000838.
Olsen, K.B., Day, S.M., Dalguer, L., Mayhew, J., Cui, Y., Zhu, J., Cruz-Atienza, V.M., Roten, D., Maechling, P., Jordan, T.H., Chourasia, A., 2009. ShakeOut-D: ground motion estimates using an ensemble of large earthquakes on the Southern San Andreas Fault with spontaneous rupture propagation. Geophys. Res. Lett. 36. doi:10.1029/2008GL036832.
Palmer, A., Rice, J.R., 1973. The growth of slip surfaces in the progressive failure of over-consolidated clay. Proc. Roy. Soc. London, Ser. A 332, 527–548.
Peyrat, S., Olsen, K.B., Madariaga, R., 2001. Dynamic modeling of the 1992 Landers earthquake. J. Geophys. Res. 106, 26,467–26,482.
Piatanesi, A., Tinti, E., Cocco, M., Fukuyama, E., 2004. The dependence of traction evolution on the earthquake source time function adopted in kinematic rupture models. Geophys. Res. Lett. 31, L04609. doi:10.1029/2003GL019225.
Pulido, N., Irikura, K., 2000. Estimation of dynamic rupture parameters from the radiated seismic energy and apparent stress. Geophys. Res. Lett. 27, 3945–3948.
Rosakis, A.J., Samudrala, O., Coker, D., 1999. Cracks Faster than the Shear Wave Speed. Science 284. doi:10.1126/science.284.5418.1337.
Spudich, P., Guatteri, M., 2004. The effect of bandwidth limitations on the inference of earthquake slip-weakening distance from seismograms. Bull. Seismol. Soc. Am. 94, 2028–2036.
Toksöz, M.N., Reilinger, R.E., Doll, C.G., Barka, A.A., Yalcin, N., 1999. Izmit (Turkey) Earthquake of 17 August 1999:First Report. Seis. Res. Ltrs. 70, 669–679.
Vallée, M., Landès, M., Shapiro, N.M., Klinger, Y., 2008. The 14 November 2001 Kokoxili (Tibet) earthquake: high-frequency seismic radiation originating from the transitions between sub-Rayleigh and supershear rupture velocity regimes. J. Geophys. Res. 113, B07305. doi:10.1029/2007JB005520.
Virieux, J., Madariaga, R., 1982. Dynamic faulting studied by a finite difference method. Bull. Seismol. Soc. Am. 72, 345–369.
Xia, K., Rosakis, A.J., Kanamori, H., Rice, J.R., 2005. Laboratory Earthquakes Along Inhomogeneous Faults: Directionality and Supershear. Science 308, 681. doi:10.1126/science.1108193.